2026 IEEE International Conference on Robotics and Automation (ICRA 2026)
June 1-5, 2026. Vienna, Austria

Design of a single-input, five-output differential actuation unit for underactuated hands

Hugo SCUDERONI
SeaTech School of Engineering
Université de Toulon
Toulon, France
hugo@scuderoni.fr

Alessandro PERINI
Department of Industrial Engineering
University of Rome Tor Vergata
Rome, Italy
alessandro.perini@students.uniroma2.eu

Matteo RUSSO
Department of Industrial Engineering
University of Rome Tor Vergata
Rome, Italy
matteo.russo@uniroma2.eu

***Abstract*—Robotic hands, prosthetics, and hand exoskeletons struggle with replicating the natural dexterity of human hands: the mechanical intelligence of our muscles can be hardly replicated with rigid actuators, while soft mechanisms compromise precision. Underactuated hand mechanisms represent a trade-off between these extremes. However, single-motor solutions, while robust and compact, generally actuate a maximum of four fingers or present critical differences in force transmission between the fingers. Here, we propose a design for a single-input, five-output differential gearbox that delivers balanced transmission thanks to a unique asymmetrical layout. This feature enables adaptive grasp control through mechanical intelligence only, providing the user with a reliable, safe, and lightweight solution for tendon-driven hand mechanisms. A preliminary 3D-printed prototype is presented to demonstrate the concept.**

***Index Terms*—underactuation, robotic hands, exoskeletons, prostheses, mechanical design,**

I. Introduction

Thanks to the intrinsic compliance and power density of our muscles, the human hand achieves a unique capability in performing complex manipulation tasks. Due to the technological limit of current actuators, robotic hands can hardly replicate this dexterity [1]. Replacing each muscle with a dedicated motor results in extremely bulky and complex systems, since our hands and wrist are actuated by 20 muscles located in the forearm and 21 muscles located in the hand itself [2]. Therefore, underactuation and differential mechanisms have been often proposed [3]–[5] to balance the trade-off between replicating human dexterity and minimizing complexity. These solutions enable the control of multiple degrees of freedom (DOFs) with fewer actuators, reducing weight and complexity while maintaining functional grasping and adaptability.

Researchers have presented several architectures to obtain underactuated human-like hand motions, aiming to minimize the number of active motors, which provide precise control but add weight, encumbrance, and complexity. These solutions have been presented for three main applications: hand prostheses, human-like robot hands, and hand exoskeletons.

Hand prostheses, such as [6]–[9], often present strategies to actuate all fingers with a reduced number of motors; however, these solutions introduce critical motion coupling among two or more fingers, losing dexterity in specific hand configurations. In contrast, solutions with at least one motor embedded in each finger, such as [10], add control complexity, bulk, and manufacturing costs. Human-like robotic hands, often designed either for humanoid robots or as end-effectors for industrial manipulators, follow similar design trends to achieve human-like grasping capabilities [11]–[13].

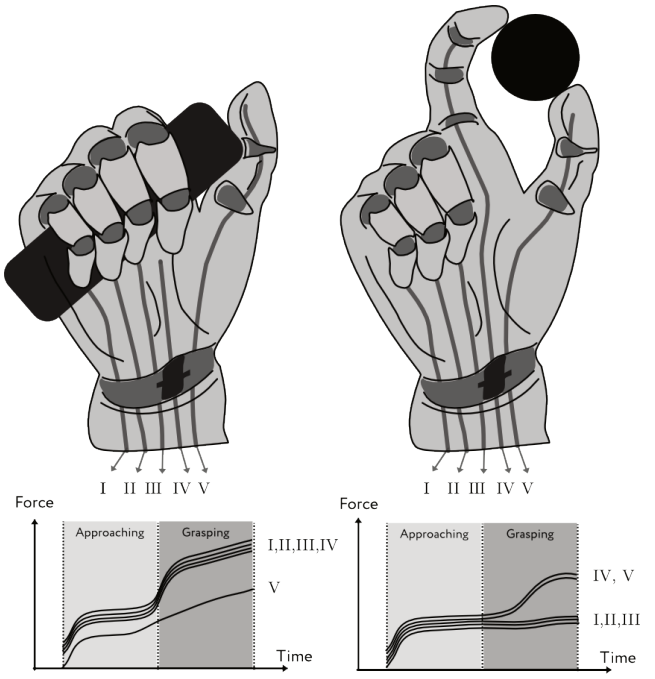

Fig. 1: A conceptual representation of force distributions when grasping objects with different shapes. If the actuation of each finger cannot adapt to this gradient, the grasp fails or the object risks being damaged.

Hand exoskeleton mechanisms generally adopt different designs, given their necessity to be worn over the user's hand rather than replacing it. For these designs, tendon-based transmission is often favoured to minimize encumbrance.

Underactuation strategies [14]–[17] are here often found together with compliant mechanisms and spring-based solutions [18]–[20], which however compromise the precision of the mechanisms as well as limit their general range of motion and operation. Conversely, differential mechanisms allow for a force/motion distribution that intrinsically adapts to dynamic loading conditions, especially when a gradient is observed between the outputs. In this way, mechanisms adaptivity to the environment and manipulated objects (see illustration in Fig. 1) is achieved without sacrificing neither precision nor motion control.

Differential mechanisms, such as planetary gearbox, generally split one input into two outputs. As such, a balanced transmission can be easily achieved with n differential stages in series as long as the number of output is equal to 2^n. Because of this limitation, many differential designs neglect one finger, usually pinky or thumb, to only actuate the other four. Several one-input, four-output gearbox examples can be found for the actuation of both prostheses and exoskeletons [6], [14]. Pulley-based differential designs, still with four outputs, have also been proposed [16]. Scaling up the differential from four to five balanced fingers, however, is extremely challenging. Additionally, pulley trees have a flat but large form factor that can be lodged inside prosthesis hands but results too large for exoskeletons and other applications, whereas gearbox-based differentials can be assembled on a single shaft with a more compact shape factor. A trivial solution could involve using a three-layered tree of differential mechanisms in series, obtaining 8 outputs and locking 3 of them; however, this solution highly increase complexity and encumbrance. A custom asymmetric gearbox could be used to avoid adding redundant or supernumerary stages, but existing examples, such as [21], are critically flawed by transmission imbalance between fingers that prevents functional operation.

This paper addresses this gap with the design, modeling, and validation of a balanced one-input, five-output differential mechanism based on planetary gears. The aim of this design is to ensure distributed force and motion control across the five fingers of a robotic hand device or hand exoskeletons, paving the way for newer tendon-driven underactuated solutions. In Section II, we present the gearbox requirements and conceptual design together with the mathematical modeling used for its dimensional synthesis. Section III presents an experimental validation of the concept with a preliminary prototype, demonstrating the balance between outputs in different operating conditions. Finally, we discuss the results to highlight the advantages and disadvantages of the proposed design and outline future developments.

II. Methodology

A. Conceptual design

The design solution presented in this paper aims at underactuating five-fingered hand mechanisms with a single motor while maintaining the capability to perform an adaptive grasp.

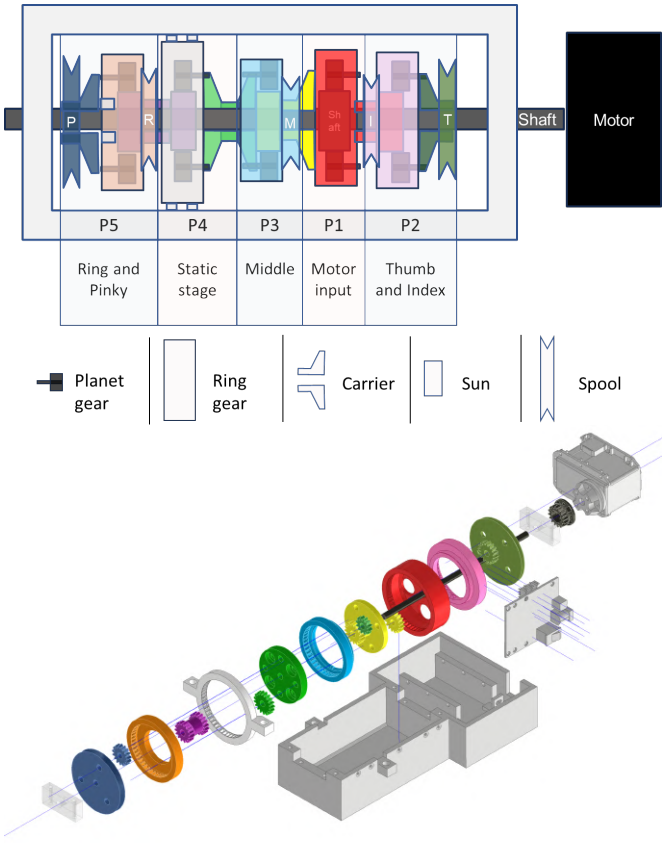

Fig. 2: Architecture of the proposed gearbox, with stage P1 connected to the motor shaft through its sun gear and distributing torques between stages P2 and P3; stage P2 splits its input from P1 into thumb and index actuation, whereas stage P3 splits its input from P1 into the middle finger actuation and the static stage P4. Stage P4 acts as static gain, transmitting motion to stage P5 that further distributes its input torque among ring finger and pinky.

The proposed actuation unit is conceived as an application-agnostic mechanism that can be applied to different kinds of robotic hand mechanisms, from humanoid hands to prosthesis and exoskeletons. To achieve this goal, we propose a gearbox with five differential stages that uses the motor shaft as individual input and five pulleys as output.

Each differential stage distributes the power and motion from one input shaft to two output shafts while allowing them to rotate at different speeds. When no additional kinematic constraint is applied, the stage balances torque between the two outputs so that the output with the least resistance moves more. In a hand mechanism, this results in fingers closing onto objects all together at first; then, once a finger makes contact, motion is automatically redistributed onto the other fingers until all of them either make contact with the object or fully close onto the hand, as in the conceptual scheme in

Fig. 1. Therefore, the mechanical intelligence of the proposed gearbox automatically adapts to the shape of the grasped object. Furthermore, the gearbox makes exoskeletons and prosthesis also intrinsically safer for patients, as higher forces due to undesired disturbances automatically redistribute onto the whole hand rather than acting on a single finger.

Designing such a differential gearbox can be achieved with a variety of mechanical solutions, from pulleys to gears. Here, we propose a solution based on cylindrical gears rotating around a single axis for compactness and miniaturization potential. The schematic of the gearbox is reported in Fig. 2, where the connection between the five stages of the mechanism are illustrated.

The main challenge in designing such a gearbox is tuning the transmission ratio of each stage so that the outputs are balanced, meaning that the motor input is equally distributed onto the five outputs when they all oppose the same resistance. If the mechanism is not balanced, the system behavior will be biased towards one or more fingers that will close before the others and end up exerting a much higher force; this behavior can result in operational failure as well as damage to the robot or the user. Previous designs either neglect this issue or exclude a finger to obtain a four-output symmetric design [14], [21]. With this paper, instead, we introduce a functional, balanced solution by carefully dimensioning the gearbox stages and compensating leftover output differences by varying tendon pulley diameters.

NOMENCLATURE

η	Balance ratio
γ	Velocity gain
λ_i	Transmission parameter, i^{th} stage, $i \in \{1, \dots, 5\}$
ω_0	Angular velocity of the input shaft
ω_I	Angular velocity of the index spool
ω_M	Angular velocity of the middle finger spool
ω_P	Angular velocity of the pinky spool
ω_R	Angular velocity of the ring finger spool
ω_T	Angular velocity of the thumb spool
ω_{ic}	Angular velocity of the carrier of the i^{th} stage
ω_{ir}	Angular velocity of the ring gear of the i^{th} stage
ω_{is}	Angular velocity of the sun gear of the i^{th} stage
D_I	Index spool diameter
D_M	Middle finger spool diameter
D_P	Pinky spool diameter
D_R	Ring finger spool diameter
D_T	Thumb spool diameter
Pi	i^{th} stage of the gearbox, $i \in \{1, \dots, 5\}$
R_c	Planetary gear ratio with carrier as output
R_r	Planetary gear ratio with ring as output
Z_r	Number of teeth of the ring gear
Z_s	Number of teeth of the sun gear

B. Modeling

The transmission characteristics of each stage P of the gearbox can be described by the Willis equation, which relates the angular velocity (ω) of the ring gear (r), carrier (c), and sun gear (s) of a planetary mechanism (see Fig. 3) to their number of teeth. The Willis equation of each stage can be written as a function of a parameter $\lambda = \frac{Z_r}{Z_s}$, equal to the ratio between the number of teeth of the ring and the sun gear of each stage, as:

$$\omega_0 = \omega_{1s} = (1+\lambda_1)\omega_{1_c} - \lambda_1\omega_{1r} \tag{1}$$
$$\omega_{1r} = \omega_{2s} = (1+\lambda_2)\omega_{2_c} - \lambda_2\omega_{2_r} \tag{2}$$
$$\omega_{1_c} = \omega_{3s} = (1+\lambda_3)\omega_{3_c} - \lambda_3\omega_{3_r} \tag{3}$$
$$\omega_{4_s} = (1+\lambda_4)\omega_{3_c} \tag{4}$$
$$\omega_{4_s} = \omega_{5s} = (1+\lambda_5)\omega_{4_c} - \lambda_5\omega_{5_r} \tag{5}$$

where the corresponding terms are connected to the spool belonging to each finger:

$$\omega_{2_c} = \omega_T \tag{6}$$
$$\omega_{2_r} = \omega_I \tag{7}$$
$$\omega_{3_r} = \omega_M \tag{8}$$
$$\omega_{5_r} = \omega_R \tag{9}$$
$$\omega_{4_c} = \omega_P \tag{10}$$

The above equations can be rewritten to obtain an implicit formulation that directly expresses the relationship between inputs and outputs, as:

$$\begin{aligned}\omega_0 = &-\lambda_1(1+\lambda_2)\omega_T + \lambda_1\lambda_2\omega_I \\ &- \lambda_3(1+\lambda_1)\omega_M - \frac{\lambda_5(1+\lambda_1)(1+\lambda_3)}{1+\lambda_4}\omega_R \\ &+ \frac{(1+\lambda_5)(1+\lambda_1)(1+\lambda_3)}{1+\lambda_4}\omega_P\end{aligned} \tag{11}$$

This equation shows how the transmission between input and output is defined by a parameter γ that only depends on system geometry:

$$\omega_0 = \gamma_T\omega_T + \gamma_I\omega_I + \gamma_M\omega_M + \gamma_R\omega_R + \gamma_P\omega_P \tag{12}$$

An asymmetric multi-output differential gearbox leads to unbalanced force/motion transmission during operation; with reference to (12), a fully balanced transmission is observed when the ratio between any two γ parameters is 1:1. When this does not happen, some output can see a large increase in one factor between force or motion and a large reduction in the other; for example, the design in [21] can get up to a 48:1 force/motion ratio between different fingers. As outlined in the Introduction, obtaining a balanced asymmetric transmission is not straightforward. A direct numerical optimization of the Willis equations of the system would not take into account manufacturing and functional constraints of the gears, such as interference and profile correction. As such, the dimensional synthesis of a five-output gearbox needs to also

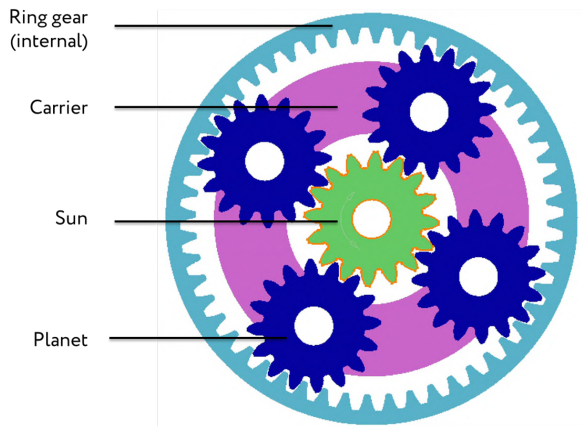

Fig. 3: Front view of a single stage of a differential mechanism with its main components: sun gear, ring gear, carrier, and planet gears. In the design, each stage receives its input from the sun gear and distributes it to two outputs on the ring gear and the carrier.

implement gear profile and inter-axis corrections. A further challenge is maintaining the entire gearbox along a single rotation axis to minimize encumbrance.

C. Mechanism synthesis

Our proposed concept has been obtained through a combination of numerical optimization and design iterations. A pure numerical optimization could not find a feasible solution for the dimensional synthesis of four serial planetary gearboxes within our manufacturing (e.g., gear profile and coupling, 3D printer tolerance, tooth strength), functional (e.g., balanced outputs, no interference, no backlash), and geometrical constraints (e.g., same axis, diameter ratio between gears smaller than 4:1). To obtain a feasible design within constraints, we here propose two design variations to a serial tree of planetary gearboxes: first, a topological change adding a passive planetary stage (P4) for gear reduction only; second, compensating leftover transmission differences by varying tendon pulley radius, rather than modifying the gearbox itself. The performance costs for the additional stage are a slight increase to the size of the system and to friction losses; the pulley radius change does not directly affect system performance but does limit the application of the proposed solution to tendon-driven systems only.

In the proposed solution, shown in Fig. 2, adopts the sun as input and the carrier and ring as outputs in each stage; thus, the transmission characteristics of each stage can be expressed as:

$$\frac{|R_c|}{|R_r|} = \frac{1+\lambda}{\lambda} = 1 + \frac{1}{\lambda} \tag{13}$$

As discussed before, we can define the balance ratio of the overall system (η) as the ratio between the maximum and minimum γ coefficients from (12).

$$\eta = \left| \frac{\max(\{\gamma_T, \gamma_I, \gamma_M, \gamma_R, \gamma_P\})}{\min(\{\gamma_T, \gamma_I, \gamma_M, \gamma_R, \gamma_P\})} \right| \tag{14}$$

This value plays a crucial role in design tuning and allows us to dimension spool diameter for further output compensation; a negative transmission ratio indicates a spool that is rotating in the opposite direction of the motor shaft and can be also compensated by winding the tendon in the opposite direction on the spool.

A preliminary optimization has been used to obtain a starting λ value of 3.25 for all the stages. Using this value as a starting point for a numerical refinement within the problem's geometrical constraints leads to a feasible solution with $\lambda_1 = \lambda_2 = \lambda_5 = 3.25$; $\lambda_3 = 2.368$; $\lambda_4 = 3.404$. Thus, the transmission of the system can be characterized with (12) as:

$$\begin{aligned} \omega_0 = &-13.81 \cdot \omega_T + 10.56 \cdot \omega_I - 10.06 \cdot \omega_M \\ &- 10.56 \cdot \omega_R + 13.81 \cdot \omega_P \end{aligned} \tag{15}$$

and the balance ratio is:

$$\eta = \left| \frac{\gamma_{max}}{\gamma_{min}} \right| = 1.37 \tag{16}$$

Once the γ coefficients for each finger are known, rather than pushing the optimization further against physical and functional constraints, we can balance system behavior by adjusting pulley geometry, as tendon tension is equal to output torque multiplied by spool diameter. This adjustment ensures that each output has a balanced force. As such, spool diameters have been changed to:

$$D_{\mathrm{P}} = D_{\mathrm{T}} = 1.37 \cdot D_{\mathrm{M}} \tag{17}$$

$$D_{\mathrm{R}} = D_{\mathrm{I}} = 1.05 \cdot D_{\mathrm{M}} \tag{18}$$

If a different distribution of force and motion is required in specific applications, these equations can be used to scale the transmission balance of the gearbox as needed. In the following tables, we summarize the final design parameters, resulting in the design in Fig. 4. The non integer λ parameters are mostly due to the profile shift needed to minimize backlash. The profile shift is needed to ensure smooth meshing of gears with a low number of teeth, and in the ring gear to adjust the overall planetary gear set size and meshing. Other corrections adopted to prevent interference include decreasing the ring tooth width according to a correction angle defining the portion of the tooth that has been suppressed.

TABLE I: General gear parameters.

Module (m)	**Pressure angle** (α)	**Gear width**	**Backlash**
1 mm	20°	4 mm	0.1 mm

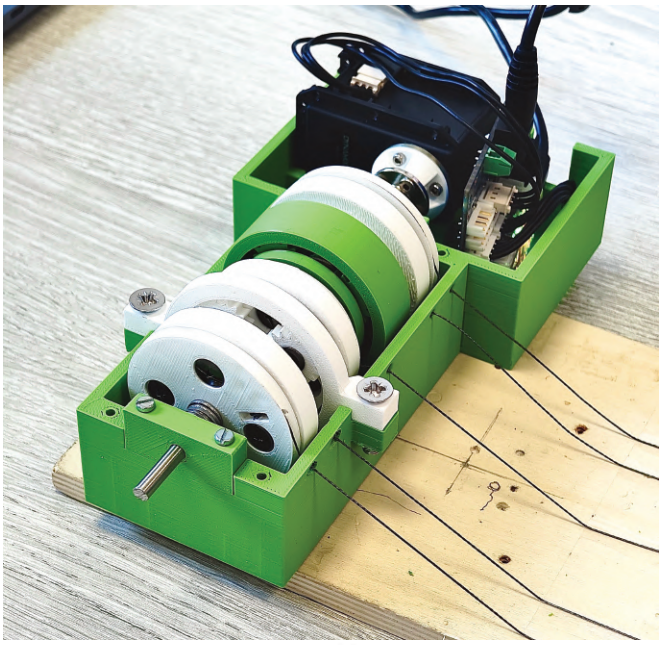

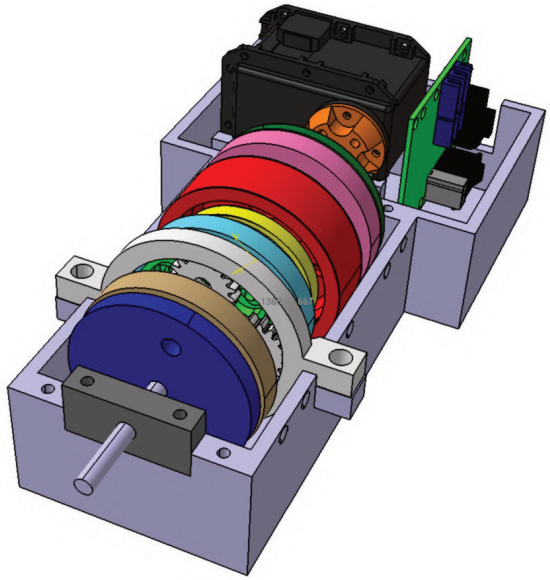

Fig. 4: CAD model of the proposed gearbox and preliminary prototype, manufactured with a FlashForge Adventurer 5M 3D printer in PLA and assembled with commercial screws, nuts, shaft, and other connectors. The input shaft is actuated by a Dynamixel MX-64T servomotor driven by a laptop through a Dynamixel U2D2 USB interface.

TABLE II: Gear correction parameters.

Set	λ	Z_r	Z_s	Z_p	x_r	x_s	x_p	**PA** (°)	**CA** (°)
P1,P2,P5	3.25	52	16	16	-0.81	0.31	0.31	0,90,180,270	0.45
P3	2.368	45	19	12	0.37	0.14	0.55	0,90,180,270	0.32
P4	3.404	51	15	17	0.16	0.37	0.26	0,87.3,180,267.3	0.4

PA: Planet Angle; CA: Correction Angle

III. Results and Discussion

The CAD model in Fig. 4 has been manufactured to validate the design. Custom parts and gears have been printed in PLA with a FlashForge Adventurer 5M; commercial components have been used to complete the assembly, as illustrated in Fig. 5. A Dynamixel MX-64T servomotor has been used to drive the input shaft of the gearbox from a laptop through a U2D2 USB interface. The resulting prototype is 196 mm long, 69 mm wide, and 70 mm high. This preliminary prototype demonstrates system operation, but overall encumbrance will be minimized in future developments with precision manufacturing on metal parts.

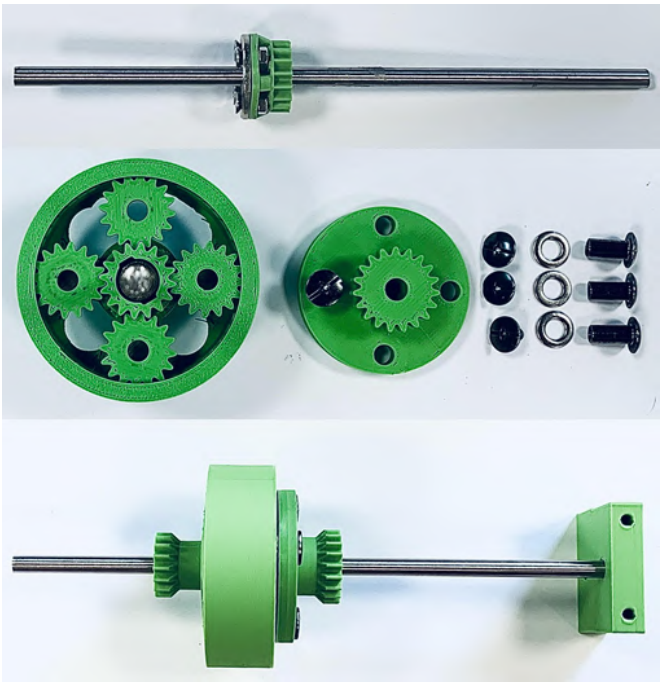

Fig. 5: Views from a partial assembly of stage P1: sun gear fixture to motor shaft, planetary stage assembly including pins and washers, and single stage assembly on motor shaft.

To validate system operation, the gearbox prototype has been tested in a fixed layout. Each tendon has been equipped with a carabiner at its free extremity and then attached to either a fixture, to lock a degree of freedom, or a spring with known stiffness, to allow for motion under a controlled force. By using equal springs for multiple tendons, the hypothesis of transmission balance can be tested, as the differential must

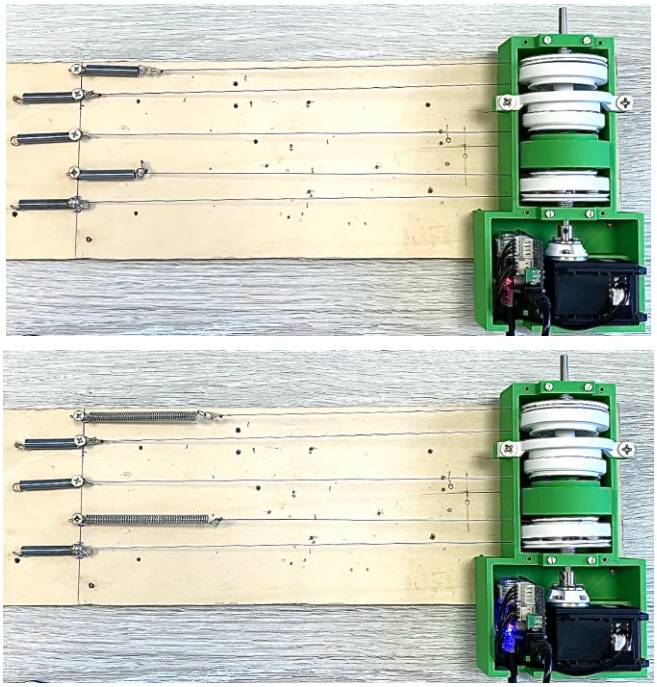

Fig. 6: Snapshots from an example experimental test with the ring finger, middle finger, and thumb actuation tendons locked in place by attaching the tendons directly to a fixturing element (infinite stiffness). The tendons for the pinky and the index are instead attached to identical springs (same stiffness). The test shows how the output force and displacements distribute adaptively between channels according to resistance, with the two springs elongating equally as the motor drives the input shaft.

distribute the force in such a way that all the springs show the same elongation.

Different configurations have been tested to validate the gearbox in different conditions with sets of ten repeated elongations. First, we tested each output individually by locking the other four with fixtures, in order to ensure that the motor can directly drive each finger. Then, different combinations of fingers have been tested to make sure that the system is balanced in partial configurations. In Fig. 6, we report the behavior of the gearbox with two outputs relative to pinky and index. This example shows how both springs elongate together, with negligible differences due to friction and manufacturing tolerances.

Finally, ten repeated tests have been carried out with all the outputs connected to springs to test the overall transmission balance of the system. Two sets of trials have been carried out: a first set included continuous elongation and shortening back to the rest position whereas in a second the springs have been driven to their limit to test the robustness of the gearbox.

The first set of trials highlighted the manufacturing limit of the 3D printed prototype, showing transmission errors especially in the release phase due to our assumption of no friction or other losses in the system. An example layout after pulling in shown in Fig. 7. The elongation of springs connected to each finger's tendon was measured and averaged to determine the traction forces. The maximum error measured was at the pinky finger with 32%, indicating a significant difference in traction forces across the system's outputs. The average relative elongation loss among the fingers was 11%. The maximum recorded loss on a single elongation was 32% for the pinky, 29% for the ring finger, 4% for the middle finger, 8% for the index, and 3% for the thumb. These values are mostly caused by cumulative friction throughout the stages and clearance/backlash due to 3D printing inaccuracies. The test in Fig. 7 clearly shows how this error stacks throughout stages, with the least resistance in the output that is closest to the motor input and the maximum loss in the furthest pulley.

Performance was further worsened in the release phase by tendon slacking. Even though the differential behavior of the mechanism intrinsically compensates for slacking by redistributing tension from the other tendons, we can still observe dynamic slacking due to friction and motion direction changes resulting into backlash.

In the last set of trials, the system has been tested up to its limits, driving the motor up to system failure. In the loading phase, the gearbox shows a linear behavior throughout its working range, as shown in the example motion/torque acquisition in Fig. 8. The linear behavior of the spring acting onto the tendon is transmitted without undesired nonlinearities throughout the gearbox despite increased system complexity. Increasing the load over the system's limit, different kinds of mechanical failure have been observed, including carabiner failure and spring plastic deformation. The gearbox and tendons showed a satisfactorily robust behavior, with no failure directly attributable to them. In case of failure at one tendon, the gearbox also showed the expected response, redistributing the excess force immediately onto the other tendons.

Overall, the proposed design represents a functional solution for a balanced asymmetric gearbox with five outputs; while the main application of this design refers to the underactuation of tendon-driven hand mechanisms, it can be adapted to any other application that requires adaptive mechanical control over a number of outputs.

IV. Conclusion

This paper introduced a balanced gearbox that adaptively distributes the torque from one input to five differential output, with the aim of underactuating hand mechanisms for robots, prostheses, and exoskeletons with a single motor controlling the flexion of all fingers. The main contributions of this work can be summarized as:

- Topological and dimensional synthesis of a one-input, five-output gearbox with planetary stages along a single

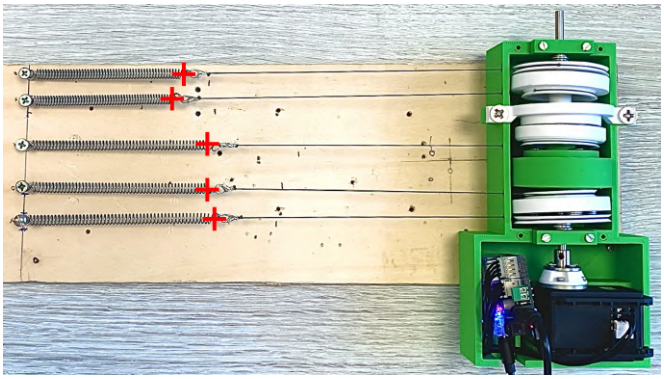

Fig. 7: Snapshots from an experimental test with all the tendons attached to identical springs (same stiffness). The test shows how the output force and displacements distribute adaptively between channels according to resistance, with springs elongating similarly as the motor drives the input shaft. Friction and manufacturing inaccuracies are highlighted by small differences in elongation: the farthest differential stage (P5) from the input (P1) shows a slightly lower elongation due to cumulative losses.

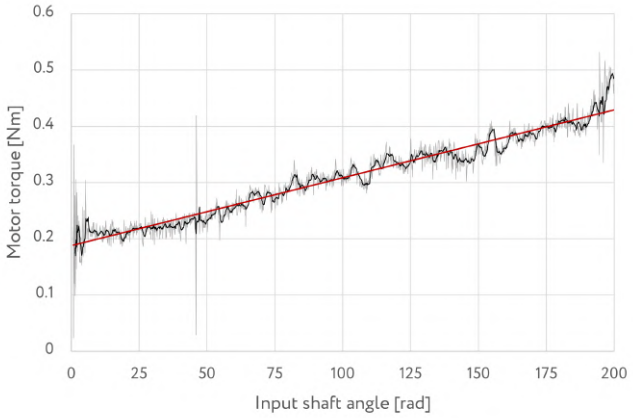

Fig. 8: Relationship between input shaft rotation and motor torque during an example elongation test, with raw data in grey, filtered data (mobile average, 10 periods) in black, and linear trend ($R^2 = 0.9231$) in red.

rotation axis, with overall mechanism architecture, preliminary sizing, and gear profile correction to maintain the design within geometrical constraints.

- Design solutions to achieve balanced transmission between outputs, including the inclusion of passive reduction stages and spool diameter compensation for tendon-driven mechanisms.
- Validation of the proposed architecture with a preliminary prototype, demonstrating balanced transmission within expected errors due to friction and manufacturing limits.

This design improves on previous works that only provide four differential outputs or are characterized by large force/motion transmission differences (approx. 48:1) between outputs. Given the limits of PLA/ABS 3D printing, future developments will focus on the miniaturization of the gearbox with precision manufacturing and steel components (from preliminary estimates, reducing the gearbox by 75% without compromising its strength) and its implementation in prosthesis, hand, and exoskeleton prototypes.

REFERENCES

[1] G. Gao, A. Dwivedi, and M. Liarokapis, "An Anthropomorphic Prosthetic Hand with an Active, Selectively Lockable Differential Mechanism: Towards Affordable Dexterity," in *2021 IEEE/RSJ International Conference on Intelligent Robots and Systems (IROS)*, Sep. 2021, pp. 6147–6152, iSSN: 2153-0866. [Online]. Available: https://ieeexplore.ieee.org/document/9636621/

[2] A. R. Sobinov and S. J. Bensmaia, "The neural mechanisms of manual dexterity," *Nature Reviews Neuroscience*, vol. 22, no. 12, pp. 741–757, Dec. 2021. [Online]. Available: https://www.nature.com/articles/s41583-021-00528-7

[3] B. He, S. Wang, and Y. Liu, "Underactuated robotics: a review," *International Journal of Advanced Robotic Systems*, vol. 16, no. 4, p. 1729881419862164, 2019.

[4] M. Dragusanu, D. Troisi, A. Villani, D. Prattichizzo, and M. Malvezzi, "Design and prototyping of an underactuated hand exoskeleton with fingers coupled by a gear-based differential," *Frontiers in Robotics and AI*, vol. 9, p. 862340, 2022.

[5] G. C. Matrone, C. Cipriani, E. L. Secco, G. Magenes, and M. C. Carrozza, "Principal components analysis based control of a multi-dof underactuated prosthetic hand," *Journal of neuroengineering and rehabilitation*, vol. 7, no. 1, p. 16, 2010.

[6] G. Gao, M. Shahmohammadi, L. Gerez, G. Kontoudis, and M. Liarokapis, "On differential mechanisms for underactuated, lightweight, adaptive prosthetic hands," *Frontiers in Neurorobotics*, vol. 15, p. 702031, 2021.

[7] H. Li, C. J. Ford, M. Bianchi, M. G. Catalano, E. Psomopoulou, and N. F. Lepora, "Brl/pisa/iit softhand: a low-cost, 3d-printed, underactuated, tendon-driven hand with soft and adaptive synergies," *IEEE Robotics and Automation Letters*, vol. 7, no. 4, pp. 8745–8751, 2022.

[8] C. Della Santina, C. Piazza, G. Grioli, M. G. Catalano, and A. Bicchi, "Toward dexterous manipulation with augmented adaptive synergies: The pisa/iit softhand 2," *IEEE Transactions on Robotics*, vol. 34, no. 5, pp. 1141–1156, 2018.

[9] D. Esposito, S. Savino, E. Andreozzi, C. Cosenza, V. Niola, and P. Bifulco, "The "federica" hand," *Bioengineering*, vol. 8, no. 9, p. 128, 2021.

[10] M. Cheng, L. Jiang, S. Fan, B. Yang, J. Dai, and H. Liu, "Development of a multisensory underactuated prosthetic hand with fully integrated electronics," *IEEE/ASME Transactions on Mechatronics*, vol. 28, no. 2, pp. 1187–1198, 2022.

[11] T. Laliberté, L. Birglen, and C. Gosselin, "Underactuation in robotic grasping hands," *Machine Intelligence & Robotic Control*, vol. 4, no. 3, pp. 1–11, 2002.

[12] S. Cheon, W. Choi, S.-R. Oh, and Y. Oh, "Development of an underactuated robotic hand using differential gear mechanism," in *2014 11th International Conference on Ubiquitous Robots and Ambient Intelligence (URAI)*. IEEE, 2014, pp. 328–334.

[13] M. Shahmohammadi and M. Liarokapis, "A series elastic, compact differential mechanism: On the development of adaptive, lightweight robotic grippers and hands," in *2021 IEEE/RSJ International Conference on Intelligent Robots and Systems (IROS)*. IEEE, 2021, pp. 6110–6116.

[14] L. Gerez and M. Liarokapis, "An underactuated, tendon-driven, wearable exo-glove with a four-output differential mechanism," in *2019 41st Annual International Conference of the IEEE Engineering in Medicine and Biology Society (EMBC)*. IEEE, 2019, pp. 6224–6228.

[15] V. Khatik and A. Saxena, "On optimal tendon routing-based design of biologically inspired underactuated hand exoskeleton for gross grasping," *IEEE Transactions on Medical Robotics and Bionics*, vol. 6, no. 2, pp. 600–617, 2024.
[16] A. Bajaj, V. Jain, P. Kumar, A. Unal, and A. Saxena, "Soft hand exoskeleton for adaptive grasping using a compact differential mechanism," in *Mechanism and Machine Science: Select Proceedings of Asian MMS 2018*. Springer, 2020, pp. 733–746.
[17] B. Kim, U. Jeong, and K.-J. Cho, "Dual-tendon routing: Tendon routing for under-actuated tendon-driven soft hand-wearable robot," *IEEE Robotics and Automation Letters*, 2025.
[18] K. Minamii and M. Yoshikawa, "A hand exoskeleton with 3d-printed compliant mechanisms to assist grasping," in *2024 46th Annual International Conference of the IEEE Engineering in Medicine and Biology Society (EMBC)*. IEEE, 2024, pp. 1–4.
[19] C. J. Nycz, T. Bützer, O. Lambercy, J. Arata, G. S. Fischer, and R. Gassert, "Design and characterization of a lightweight and fully portable remote actuation system for use with a hand exoskeleton," *IEEE Robotics and Automation Letters*, vol. 1, no. 2, pp. 976–983, 2016.
[20] Q. Meng, Z. Shen, Z. Nie, Q. Meng, Z. Wu, and H. Yu, "Modeling and evaluation of a novel hybrid-driven compliant hand exoskeleton based on human-machine coupling model," *Applied Sciences*, vol. 11, no. 22, p. 10825, 2021.
[21] A. Perini and M. Russo, "Design of an adaptive tendon-driven hand exoskeleton for stroke rehabilitation," in *2025 IEEE 8th International Conference on Soft Robotics (RoboSoft)*. IEEE, 2025, pp. 1–8.